Finite-Element Simulation of Moving Induction Heat Treatment

K.F. Wang, S. Chandrasekar, and H.T.Y. Yang

An efficient finite-element procedure with a remesh scheme has been developed for the analysis of the moving induction heat treatment process, wherein relative motion occurs between the coil and the workpiece. In this procedure, the magnetic field is first simulated by using an updated mesh that tracks the moving coil position; the moving heat source within the workpiece material is derived from the magnetic field. The heat equation is then solved to obtain the temperature field created by the heat source. The procedure has been applied to calculate the temperature distributions in 1080 carbon steel cylinders during induction heating. The calculations have been validated by comparison with analytical solutions for the temperature distribution obtained using Green's function methods. Finally, the temperature, residual stress, and microstructure distributions in quenched 1080 steel cylinders have been obtained using the finite-element procedure. Quenching of the heated cylinders, by both a moving cooling ring and a stationary liquid bath, has been analyzed. The finite-element procedure presented incorporates temperature-dependent material properties, phase transformations occurring in the 1080 steel, the change in magnetic permeability of the 1080 steel at the Curie temperature, and an elastoplastic stress model based on a mixed hardening rule. The simulation results demonstrate that the finite-element procedure could be applied to a variety of moving induction heat treatment problems to determine the residual stress and microstructure distributions in the heat-treated component. It also could be used in the design of process parameters and coils.

Keywords
finite-element analysis, induction hardening, process modeling

1. Introduction

TWO types of induction heat treatment processes are commonly used in industry: stationary induction heat treatment and moving induction heat treatment. In stationary induction hardening, the workpiece—which is made of an electrically conducting material—is stationary and is surrounded by stationary coils carrying an alternating electric current. No relative motion occurs between the coils and the workpiece. The electromagnetic field produced by the current-carrying coils induces eddy currents in the workpiece, which thus is heated resistively. After the workpiece has attained a suitable temperature, it is quenched; workpiece hardness and microstructure change during this heating and quenching cycle due to phase transformations. Residual stresses also are introduced into the material.

In moving induction heat treatment, relative motion occurs between the coil and the workpiece during induction heating, and the workpiece may be quenched by a moving cooling ring. As in the stationary process, residual stresses are introduced into the workpiece along with hardness and microstructural changes. Moving induction heat treatment is commonly used to harden piston pins, crankshafts, and camshafts.

Several computational and analytical studies have been made of stationary induction heat treatment. Dodd and Deeds (Ref 1) obtained analytical solutions for induction heating problems by assuming a constant permeability. Subsequently, finite-element methods were used by Donea et al. (Ref 2) and Chari (Ref 3) to obtain the electromagnetic vector potential for axisymmetric and two-dimensional problems. The calculation of residual stress and hardness in an infinitely long cylinder produced by induction heat treatment was presented by Melander (Ref 4). More recently, efficient finite-element simulation procedures have been developed and validated to simulate the stationary induction heat treatment of workpieces having axisymmetric or two-dimensional geometry (Ref 5). A detailed review of the principles and applications of induction heat treatment is also given in Ref 5.

The literature pertaining to the simulation of moving induction heat treatment is quite limited. The induction heat treatment of a moving, infinitely long cylinder by a stationary coil has been analyzed by Melander (Ref 6) using finite-element and finite-difference methods. In this analysis, the material properties of relevance for calculating the magnetic field were assumed to be temperature independent and the geometry of the workpiece was limited to that of an infinitely long cylinder. Furthermore, the heat conduction equation was solved assuming steady-state conditions, and a one-dimensional model was used in the residual stress analysis. Such a model is based on the assumption that the temperature distribution within the moving cylinder has reached its steady-state condition.

In the present study, a finite-element procedure has been developed and applied to model the magnetic and temperature fields and the microstructure and thermal stress evolution in moving induction heat treatment processes. The finite-element procedures are not limited to infinitely long cylinders but can simulate the heat treatment of axisymmetric workpieces of finite length or of two-dimensional geometry. The simulation results have been validated by comparison with analytical solutions for the magnetic and temperature fields in a variety of moving induction heating problems.

K.F. Wang and **S. Chandrasekar**, Purdue University, West Lafayette, IN 47907, USA, **H.T.Y. Yang**, University of California

2. Computational Model

2.1 *Analysis of the Magnetic Field*

To estimate the heat sources generated within the material during induction heating, it is first necessary to derive the magnetic vector potential in the workpiece due to a current flowing through the induction coil. This requires solution of Maxwell's electromagnetic field equations. In terms of the magnetic vector potential (**A'**) (Ref 7),

$$\nabla \times (\frac{1}{\mu} \nabla \times A') = -\sigma \frac{\partial A'}{\partial t} + J'_0 \qquad \text{(Eq 1)}$$

where $J'_0 = -\sigma \nabla \Phi$ is the source current density. During induction heating, the current in the coil is sinusoidal with a frequency ω, so that

$$J'_0 = J_0 e^{j\omega t} \qquad \text{(Eq 2)}$$

Since **A'** is expected to vary sinusoidally with time, $A' = A'' e^{j(\omega t + \varphi)} = A e^{j\omega t}$. For induction heating problems, $\nabla \cdot A = 0$ (Ref 7) and Eq 1 becomes

$$\frac{1}{\mu} \nabla^2 A - j\omega\sigma A - \nabla \left(\frac{1}{\mu}\right) \times (\nabla \times A) + J_0 = 0 \qquad \text{(Eq 3)}$$

For the axisymmetric case, the only nonzero component of the vector potential is $A_\theta(r,z)$. On dropping the θ subscript, Eq 3 becomes

$$\frac{1}{\mu}\left(\frac{\partial^2 A}{\partial r^2} + \frac{1}{r}\frac{\partial A}{\partial r} + \frac{\partial^2 A}{\partial z^2} - \frac{A}{r^2}\right) - j\omega\sigma A + \frac{\partial (1/\mu)}{\partial r}\left(\frac{1}{r}\frac{\partial rA}{\partial r}\right)$$

$$+ \frac{\partial (1/\mu)}{\partial z}\frac{\partial A}{\partial z} + J_0 = 0 \qquad \text{(Eq 4)}$$

After discretization, the general form of the finite-element equation is obtained for each element as

$$\{[k]^e + [l]^e\}\{A\} = \{F^e\} \qquad \text{(Eq 5)}$$

where

$$k^e_{ij} = \int\int_{v^e} \frac{2\pi}{\mu}\left(\frac{\partial N_i}{\partial r}\frac{\partial N_j}{\partial r} + \frac{\partial N_i}{\partial z}\frac{\partial N_j}{\partial z}\right) r dr dz$$

$$l^e_{ij} = \iint_{v^e} 2\pi \left(\frac{1}{\mu r^2} + j\omega\sigma\right) N_i N_j \, r dr dz$$

$$F^e_i = \iint_{v^e} 2\pi J_0 N_i \, r dr dz + \int_{S^e} \frac{1}{\mu} N_i \frac{\partial A}{\partial n} dS$$

and N_i is the shape function at node i.

In the formulation, the permeability μ is assumed to be constant within an element but may vary from one element to another. Also, the permeability could in general depend on temperature.

2.2 *Temperature Analysis*

The determination of the temperature field in moving induction heat treatment requires an analysis of the heat source produced by the moving coil. Consider a distributive heat source of strength $\dot{g}$ moving along the z axis with a velocity V, as shown in Fig. 1(a). The energy equation for this problem is

$$\frac{1}{r}\frac{\partial}{\partial r}\left(kr\frac{\partial T(r,z,t)}{\partial r}\right) + \frac{\partial}{\partial z}\left(k\frac{\partial T(r,z,t)}{\partial z}\right)$$

$$+ \dot{g}(r, z - z_0 - Vt, t) = \rho C_p \frac{\partial T(r,z,t)}{\partial t} \qquad \text{(Eq 6)}$$

with boundary conditions

$$\frac{\partial T(0,z,t)}{\partial r} = 0$$

(BC)

$$k\frac{\partial T(a,z,t)}{\partial r} + h[T(a,z,t) - T_{sur}] = 0$$

and initial condition

$$T(r,z,0) = T_0 \text{ (IC)}$$

where k is thermal conductivity, ρ is density, C_p is specific heat, h is the convection coefficient, and T_{sur} and T_0, respectively, are the temperature of the surroundings and the initial temperature of the cylinder.

The heat source induced by the moving cell is given by:

$$\dot{g}(r,\xi) = \frac{\sigma\omega^2 A(r,\xi) A^*(r,\xi)}{2} \qquad \text{(Eq 7)}$$

where $\mathbf{A}^*(r,\xi)$ is the complex conjugate of the magnetic vector potential **A** at a given point, ξ is the distance of a given point along the axis from the coil center (i.e., $\xi = z - z_0 - Vt$ [see Fig. 1a], and z_0 is the axial coordinate that specifies the initial position of the coil.

The calculation of the temperature field within the workpiece can now be carried out in a fixed coordinate system (r, z) that is attached to the stationary workpiece or in a moving coordinate system (r, ξ) that is fixed to the moving coil.

2.2.1 Temperature Analysis in the Fixed Coordinate System

If a fixed coordinate system is used, the finite-element formulation for the moving induction heating problem is the same as that for the stationary induction heat treatment (Ref 5). How-

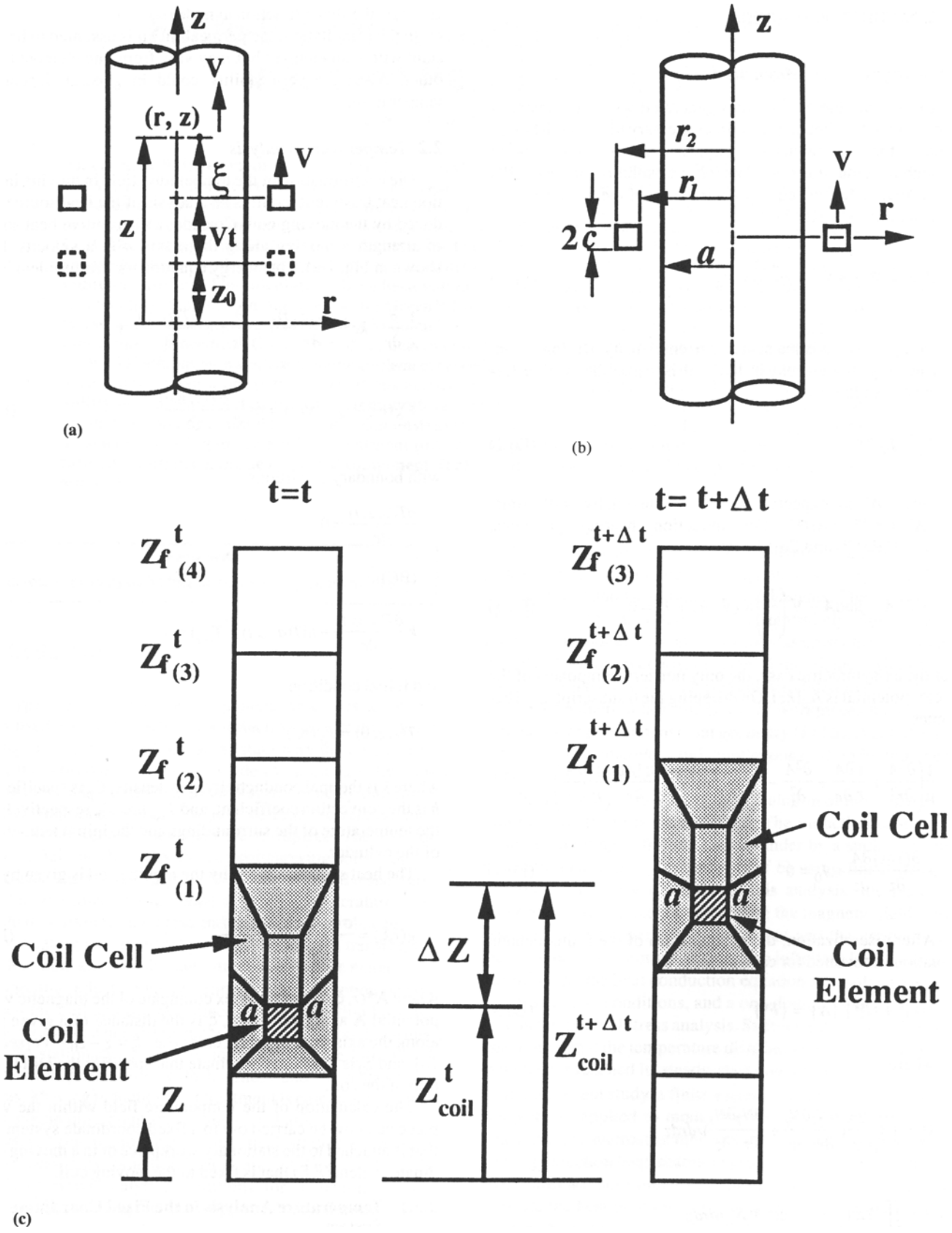

Fig. 1 (a) Coordinate system within an infinitely long cylinder heated by a moving coil. (b) Geometry of the cylinder and coil system. (c) Finite-element mesh for the moving coil showing coil cell

ever, it is suggested that an updated mesh that includes the new position of the coil element be used to more efficiently describe the moving heat source at each time step. It is also suggested that the elements on the boundary of the cylinder that are subjected to a cooling flux due to convection heat transfer be updated.

2.2.2 Temperature Analysis in the Moving Coordinate System

The heat equation can also be formulated in a moving coordinate system that moves at the same speed as the coil. The moving coordinate system offers two advantages: The same mesh can be used at each time step, and elements that are subjected to the convection heat transfer do not change.

The drawbacks of this analysis procedure are reflected when microstructures and residual stresses must be calculated. Calculation of these factors depends on temperature and stress histories, which thus must be tracked at every point within the material. The mapping of the data from the moving to the fixed coordinate system that is necessary for this purpose is computationally intensive. Another drawback of this analysis procedure is that it can be applied only to infinitely long workpieces.

2.3 *Microstructure Calculation*

The calculation of the microstructure was carried out using the formulation described by Wang et al. (Ref 8). A typical steel microstructure is composed of several phases. In the finite-element formulation, the material properties, P, at a Gauss point were assumed to be a linear combination of the corresponding properties, P_i, of each phase weighted proportional to the volume fraction, F_i, of that phase present at that point. Thus any material property, P, of the solid can be written as:

$$P(F_i,T) = \sum_i P_i(T)F_i \qquad \text{(Eq 8)}$$

where the summation is carried out over all the phases present.

The kinetics of the diffusion transformations (i.e., nonmartensitic) are described in the formulation by the following Avrami-type equation (Ref 9, 10):

$$F_i = 1 - \exp[-C_i(T)\theta^{N_i(T)}] \qquad \text{(Eq 9)}$$

where $C_i(T)$ and $N_i(T)$ are material parameters that are derived from the isothermal transformation diagram for the material, and θ is the transformation time for any phase. The calculation of these parameters for 1080 carbon steel, the material of interest to this study, is described by Fernandes et al. (Ref 11) and by Wang et al. (Ref 5).

The fraction F_m of martensite formed at a given temperature was estimated by the Koistinen-Marburger law (Ref 12):

$$F_m = [1 - \exp(-\bar{\alpha}(T_{ms} - T))](1 - \sum_i F_i) \qquad \text{(Eq 10)}$$

where $\bar{\alpha} = 1.10 \times 10^{-2}\,K^{-1}$, T_{ms} is the martensite start temperature, and the summation is over all the phases present, excluding martensite. The martensitic transformation is not diffusion controlled; therefore, its evolution equation (Eq 10) is different from that for the pearlitic transformation (Eq 9). Further details of the formulation can be found in Ref 8.

2.4 *Remesh Scheme*

In order to predict the residual stresses and microstructures, an updated mesh is suggested for use in the fixed coordinate system to model the moving coil at each time step. It is also suggested that the element numbers corresponding to the workpiece surfaces that are subjected to the heat flux of the cooling rings be updated. A finite-element remesh scheme has been developed to model the moving coil. The scheme is based on the shifting of a small group of elements referred to as a "coil cell" (Fig. 1 and 2).

The remeshing scheme is applied to a part of the mesh that includes the elements lying along the coil path. The boundary of this strip is *ijkl*, as shown in Fig. 5. Elements outside this strip are not modified. In this remeshing process, the total number of nodes and elements is kept constant.

The updating of the elements within the strip (coil path) is described by the following algorithm (Fig. 1c). These notations are used in describing the algorithm:

- Z_{coil}: z coordinate of the upper boundary of the coil element
- ΔZ: distance moved during the time interval Δt
- $Z_{f(i)}$: z coordinate of the lower boundary of the elements ahead of the coil cell
- N: number of elements through which the coil cell moves during an increment of Δt
- C_{min}: minimum allowable distance to avoid excessive distortion of the mesh

1. Update the coil position:

$$Z^{t+\Delta t}_{coil} = Z^t_{coil} + \Delta Z \qquad \text{(Eq 11)}$$

2. Determine the number of elements through which the coil cell passes. Find the minimum value of i that satisfies the equation $Z^t_{f(i)} - Z^{t+\Delta t}_{coil} > C_{min}$; then, N is equal to $i - 1$. In the present analysis, C_{min} was set equal to one-fourth the length of the coil cell.
3. Determine whether the element numbers and nodal numbers need to be updated. If $N = 0$, the coil cell does not move forward. The element numbers and nodal numbers at time $t + \Delta t$ remain the same as that at time t. The coordinate values on the outer boundaries of the cell do not change. The only change that must be made is to update the coordinate values of the nodal points within the coil cell. This is due to the movement of the coil element within the coil cell. If $N \geq 1$, the coil cell has moved through N elements. In this case, the upper boundary of the coil cell is aligned to the position $Z^t_{f(N+1)}$. N elements below the coil cell are recreated. The nodal numbers, element numbers, and coordinate values are updated. Figure 2 shows the movement of the coil cell for the special case of $N = 1$.

During the updating procedure, the following method is used for renumbering the nodal points. If the coil cell has

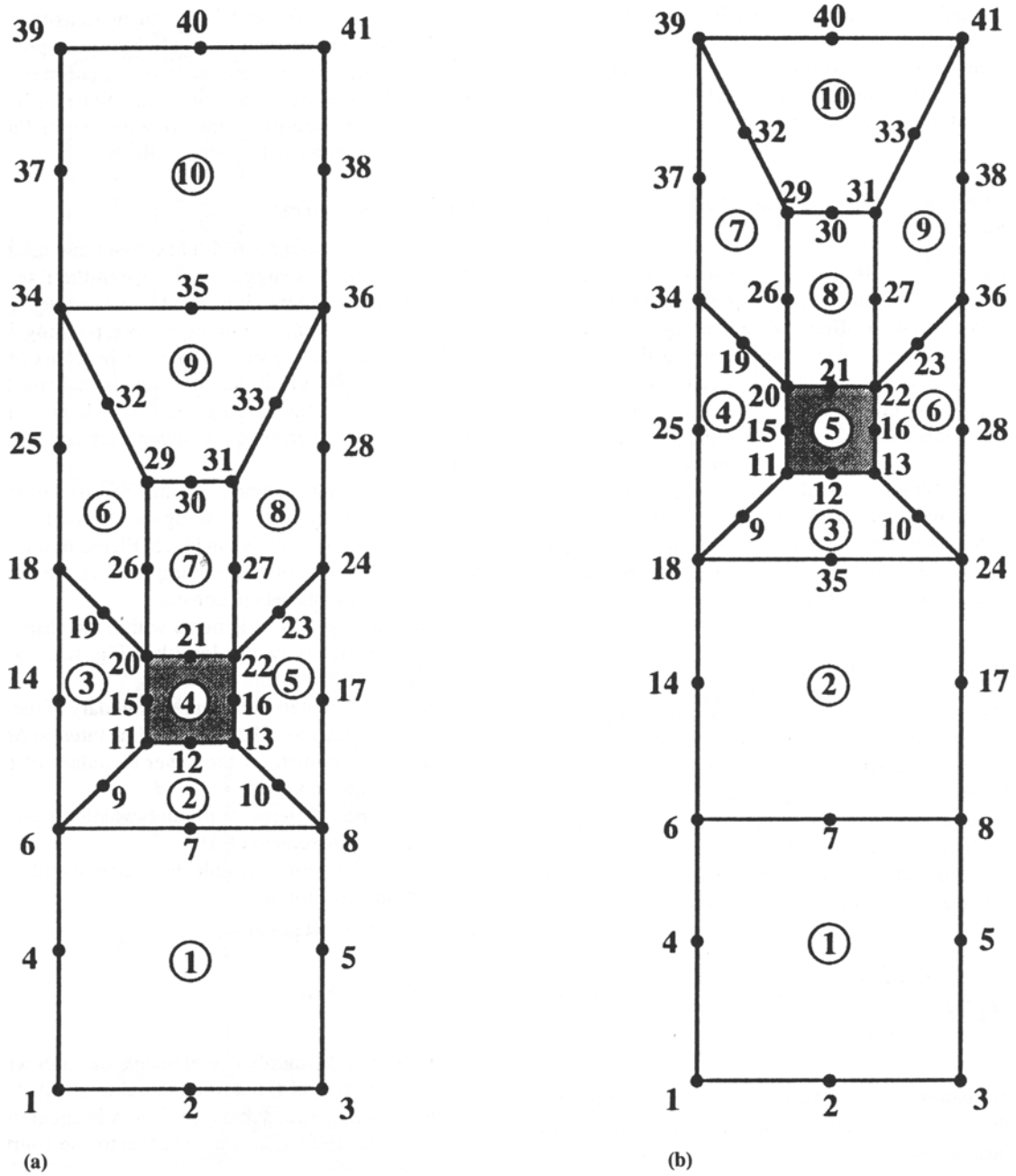

Fig. 2 Remesh scheme for the moving coil element

passed through N elements, then renumbering is done through N stages. In other words, it is assumed that the coil cell passes through a single element during a stage and nodal point numbers are modified during that stage. When the cell moves through an element during a particular stage, a new element is created below the coil cell (see Fig. 2). For this new element, the nodal point number of the middle point on the upper boundary is assigned the value of the nodal number of the middle point on the upper boundary of the coil cell at the previous stage. The nodal point numbers at the boundaries of the strip as well as within the coil cell are the same as that of the previous stage.

This algorithm is illustrated by a simple example in Fig. 2. As the coil passes through an element, a new element (2) is created. For this element (2) (Fig. 2b), the node at the midpoint of the upper boundary is numbered 35, which is the same as that of the node at the midpoint of the upper boundary of the coil in the previous stage (Fig. 2a).

2.5 *Stress Analysis*

A thermoelastic-plastic model that incorporated temperature-dependent material properties was used in the stress analysis of quenching. The von Mises yield function, with plastic

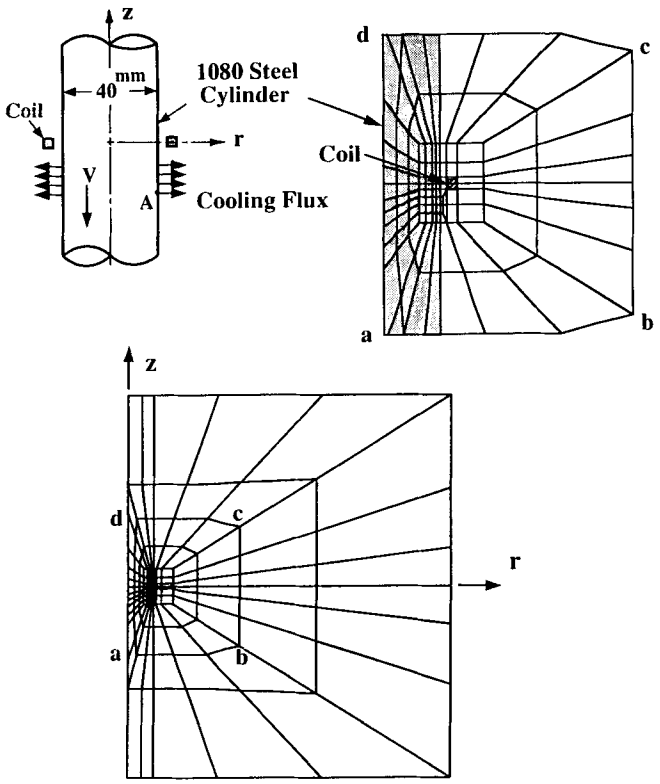

Fig. 3 Geometry and finite-element mesh for an infinitely long 1080 steel cylinder heated by a moving coil and quenched by a moving cooling flux

flow being controlled by a kinematic hardening rule, was used. The formulation of this thermoelastic-plastic model has been described in detail by Wang et al. (Ref 8).

3. Applications

In this section, several moving induction heat treatment problems are analyzed using the finite-element procedure described in section 2. Calculation of the temperature, residual stress, and microstructure distributions is emphasized.

3.1 *Induction Heat Treatment of an Infinitely Long Cylinder Heated by a Moving Coil and Quenched by a Moving Cooling Ring*

A 1080 steel cylinder, 40 mm in diameter and at an initial temperature of 25 °C, is heated by a moving coil with an inner diameter of 44 mm and a cross-sectional area of 4 by 4 mm^2 (Fig. 3). The coil is assumed to move with a constant velocity of 2.5 mm/s. First, analytical solutions for the moving heat source problem are derived using a Green's function method in section 3.1.1. Next, the temperature field is obtained using a finite-element procedure based on the moving coordinate system. In the finite-element solution, the moving cooling ring is modeled as a constant-band cooling flux. The simulation of the temperature field and its comparison with the analytical solution are discussed in section 3.1.2. Finally, the complete heat treatment process is simulated using the finite-element method with the remesh scheme based on the fixed coordinate system.

3.1.1 Analytical Solutions for Moving Heat Source Problems in Induction Heat Treatment

For an infinitely long cylinder of radius a subjected to a distributed heat source $\dot{g}(r, z, t)$, the energy equation in cylindrical coordinates is

$$\frac{\partial^2 T}{\partial r^2} + \frac{1}{r}\frac{\partial T}{\partial r} + \frac{\partial^2 T}{\partial z^2} + \frac{1}{k}\dot{g}(r, z, t) = \frac{1}{\alpha}\frac{\partial T}{\partial t} \qquad \text{(Eq 12)}$$

with boundary conditions

$$\frac{\partial T}{\partial r} = 0 \quad r = 0$$

$$\frac{\partial T}{\partial r} + HT = 0 \quad r = a$$

$$\frac{\partial T}{\partial z} = 0 \quad z = \pm\infty$$

and initial condition

$$T = T_0 \quad t = 0$$

where $H = h/k$ and h, k, and α are the convection heat-transfer coefficient, thermal conductivity, and thermal diffusivity, respectively.

The Green's function for this problem—that is, the solution for the temperature when a delta function heat source, $1/\alpha\,\delta(r - r')\delta(z - z')\delta(t - \tau)$, is imposed over a circle at (r', z')—is given by:

$$G(r, z, t \mid r', z', \tau) = \sum_{m=1}^{\infty} \frac{B_m^2 J_0(\beta_m r') J_0(\beta_m r)}{(\beta_m^2 a^2 + H^2 a^2)[J_0(\beta_m a)]^2}$$

$$\times \frac{1}{\sqrt{\pi\alpha(t - \tau)}} e^{\frac{-(z - z')^2}{4\alpha(t - \tau)}} e^{-\alpha\beta_m^2(t - \tau)} \qquad \text{(Eq 13)}$$

where the β_m terms are the positive roots of the equation $\beta_m J_1(\beta_m a) + HJ_0(\beta_m a) = 0$. This solution is for the case where k and α are constant.

The basic Green's function solution in Eq 13 can be applied to a variety of moving heat source problems. Applications related to the moving induction heat treatment of an infinitely long cylinder are described here for three cases.

3.1.1.1 *Moving Ring Source*

The heat source $\dot{g}$ in Eq 12, for a ring source of strength Q (W/m) initially at (r_0, z_0) and moving with a velocity V, can be written as:

$$\dot{g}(r,z,t) = Q\delta(r - r_0)\delta(z - z_0 - Vt)$$

The temperature within the cylinder is then obtained by integrating the Green's function of Eq 13 as:

$$T(r,z,t) = T_0 + \frac{\alpha}{k}\int_{\tau=0}^{t}\int_{-\infty}^{\infty}\int_{0}^{a} r'G(r,z,t|r',z',\tau)\cdot\dot{g}(r',z',\tau)dr'dz'd\tau$$

$$= T_0 + \frac{\alpha Q}{k}\sum_{m=1}^{\infty}\frac{\beta_m^2 J_0(\beta_m r_0)J_0(\beta_m r)}{(\beta_m^2 a^2 + H^2 a^2)[J_0(\beta_m a)]^2}$$

$$\times\int_0^t \frac{1}{\sqrt{\pi\alpha(t-\tau)}} e^{\frac{-(z-z_0-V\tau)^2}{4\alpha(t-\tau)}} e^{-\alpha\beta_m^2(t-\tau)}d\tau \qquad \text{(Eq 14)}$$

3.1.1.2 *Moving Band Source on the Surface of the Cylinder*

If $dQ = qdz$, where $q(W/m^2)$ is the strength of a band source, the temperature within the cylinder subjected to such a source on the surface located initially at (a,z_0) can be obtained by integrating the ring-source solution of Eq 14 as:

$$T(r,z,t) = T_0 + \frac{\alpha q}{k}\sum_{m=1}^{\infty}\frac{\beta_m^2 J_0(\beta_m r)}{(\beta_m^2 a^2 + H^2 a^2)J_0(\beta_m a)}$$

$$\times\int_0^t \frac{1}{\sqrt{\pi\alpha(t-\tau)}} e^{-\alpha\beta_m^2(t-\tau)}\int_{-c}^{c} \frac{e^{-(z-z_0-\xi-V\tau)_2}}{4\alpha(t-\tau)}d\xi d\tau$$

$$= T_0 + \frac{a\alpha q}{k}\sum_{m=1}^{\infty}\frac{\beta_m^2 J_0(\beta_m r)}{(\beta_m^2 a^2 + H^2 a^2)J_0(\beta_m a)}\times\int_0^t e^{-\alpha\beta_m^2(t-\tau)}$$

$$\times\left\{\text{erf}\left[\frac{z-z_0-Vt+d+V(t-\tau)}{2\sqrt{\alpha(t-\tau)}}\right]\right. \qquad \text{(Eq 15)}$$

$$\left. - \text{erf}\left[\frac{z-z_0-Vt-d+V(t-\tau)}{2\sqrt{\alpha(t-\tau)}}\right]\right\}d\tau$$

where d is the half-width of the band. This equation can be used to model a moving cooling ring that induces a band flux on the surface of the cylinder.

3.1.1.3 *Moving Distributed Source*

If an infinitely long cylinder is heated by a distributed heat source moving with velocity V, with $dQ = \dot{g}(r,z,t)drdzdt$ and $\dot{g}$ (W/m^3) is the strength, the temperature field within the cylinder is given by:

$$T(r,z,t) = T_0$$

$$+\frac{\alpha}{k}\int_0^t \frac{1}{\sqrt{\pi\alpha(t-\tau)}}\int_{-\infty}^{\infty} e^{\frac{-(z-z')^2}{4\alpha(t-\tau)}}\int_0^a r'\dot{g}(r',z'-z_0-V\tau,\tau)$$

$$\times\sum_{m=1}^{\infty}\frac{\beta_m^2 J_0(\beta_m r')J_0(\beta_m r)}{(\beta_m^2 a^2 + H^2 a^2)[J_0(\beta_m a)]^2} e^{-\alpha\beta_m^2(t-\tau)}\, dr'dz'd\tau$$

(Eq 16)

During induction heating, the distributed heat source produced by the magnetic field can be calculated from the magnetic vector potential using Eq 7. When the properties of the workpiece material are assumed to be constant, the governing differential equation in cylindrical coordinates for the magnetic vector potential **A** is

$$\frac{\partial^2 A}{\partial r^2} + \frac{1}{r}\frac{\partial A}{\partial r} + \frac{\partial^2 A}{\partial z^2} - \frac{A}{r^2} - j\omega\mu\sigma = 0 \qquad \text{(Eq 17)}$$

The equation can be solved for the appropriate boundary conditions of induction heating (see Ref 5 for the complete solution). The magnetic vector potential within an infinitely long cylinder due to current flow in the single coil shown in Fig. 1(b) is

$$A(r,z) = \frac{\mu_0 J_0}{\pi}\int_0^\infty \frac{1}{D(\eta)} F(\eta,r_1,r_2)I_1(\eta_1 r)Z(\eta,z)d\eta \qquad \text{(Eq 18)}$$

where

$$D(\eta) = \frac{1}{\mu_r}\eta_1 a I_0(\eta_1 a)K_1(\eta a) + \eta a I_1(\eta_1 a)K_0(\eta a)$$

$$+ (1 - \frac{1}{\mu_r})\, I_1(\eta_1 a)K_1(\eta a)$$

$$\mu_r = \frac{\mu}{\mu_0};\quad \eta_1 = \sqrt{\eta^2 + j\omega\mu\sigma}$$

$$F(\eta,r_1,r_2) = \int_{r_1}^{r_2} r_0 K_1(\eta r_0)dr_0$$

$$Z(\eta,z) = \frac{1}{\eta}[\sin\eta(c-z) + \sin\eta(c+z)]$$

Here J_0 is the source current density in the coil and K_0, K_1, I_0, and I_1 are the appropriate modified Bessel functions in the usual notation; and c is the half-width of the coil.

3.1.2 Finite-Element Solution Based on the Moving Coordinate System

The induction heating of the infinitely long 1080 steel cylinder (Fig. 3) was simulated by the finite-element method with a mesh in the moving coordinate system. A mesh with 154 isoparametric eight-node axisymmetric elements was used to model the entire space, including the cylinder and the coil, as shown in Fig. 3. The cooling boundary due to the cooling ring was modeled by a band (cooling) flux of strength 3.0×10^6 W/m^2. The center of the band was at $z = -6.103$ mm, and the width of the band flux was 8.205 mm. The source current density and its frequency were $1.38 \times 10^{10} A/m^2$ and 60 Hz, respectively. For comparison of the finite-element solution with the analytical solution, the material properties of the workpiece material were assumed to have constant values of 3×10^6 mho/m, 7500 kg/m^3, 650 J/kg·K, and 35 W/m·K, respectively, for the electrical conductivity, density, specific heat, and thermal conductivity.

The temperature-time history on the surface of the cylinder along a circle located at a distance of 7.17 mm below the coil center was calculated using the finite-element method for two cases: (1) induction heating without cooling and (2) induction heating followed by quenching with a cooling ring. Figure 4 compares these calculated temperature histories with those obtained using the Green's function method; the values exhibit excellent agreement.

Three different finite-element meshes (128, 154, and 256 elements, respectively) were used. Although the 128-element results compared favorably with the analytical curves in Fig. 4, some small differences existed. The 154-element mesh was sufficiently fine that its results did not differ from the 256-element results.

3.1.3 Finite-Element Solution with the Remesh Scheme

The induction heating of the infinitely long 1080 steel cylinder was also analyzed using a remesh scheme based on the fixed coordinate system. The coordinate system was fixed on the cylinder, and each nodal point within the cylinder represented a particular point in the material. The entire space comprising the infinitely long cylinder and the moving coil was modeled by a mesh of 316 isoparametric eight-node elements, in which the coil element was moved at each time step. The cylinder geometry and the mesh are shown in Fig. 5.

Figure 6 shows the temperature-time histories at three points—*D*, *D'*, and *D''*—on the surface of the cylinder (locations of these points are shown in Fig. 5) during induction heating determined using both the finite-element method and Green's function solutions. In this comparison, the material properties of the cylinder, source current density, and frequency of the current in the coil were assumed to be the same as those in the previous example. Again, excellent agreement exists between the finite-element and the analytical solutions for the temperature field.

Finally, the finite-element procedure was applied to simulate the complete heat treatment cycle involving induction heating followed by quenching in water from a moving cooling ring (Fig. 5). The heat-transfer boundary due to the moving cooling ring was updated at each time step. The convection heat-transfer coefficient for water quenching was assumed to depend on temperature, and the values used were the same as those used by Buchmayr and Kirkaldy (Ref 13). The width of the cooling band was 300 mm, with the upper boundary of the band located at a distance of 20 mm below the coil center. The cylinder surfaces not exposed to the cooling band were subjected to air cooling during the heating and quenching process. The convection coefficient for air cooling was assumed as 200 $W/m^2 \cdot K$. The physical and mechanical properties of the cylinder material were assumed to be temperature dependent and the same as those used by Wang et al. (Ref 5).

Figure 7 shows the calculated temperature-time histories at six points in the cylinder. The locations of these points are given in Fig. 5. The temperature histories at points A and D show some transient response, whereas the results at those points farther away from the initial coil position (namely, B, C, E, and F) approach the steady-state solution (Fig. 7). Figure 8 shows the microstructure distribution in the outer region ($4 < r < 20$ mm) of the cylinder where the austenite transformation

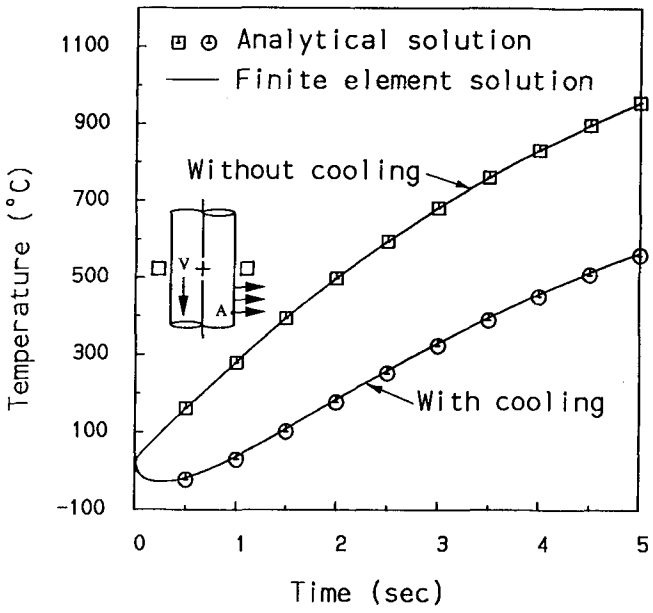

Fig. 4 Temperature-time histories on the surface of the infinitely long cylinder at a distance of 7.17 mm below the coil center

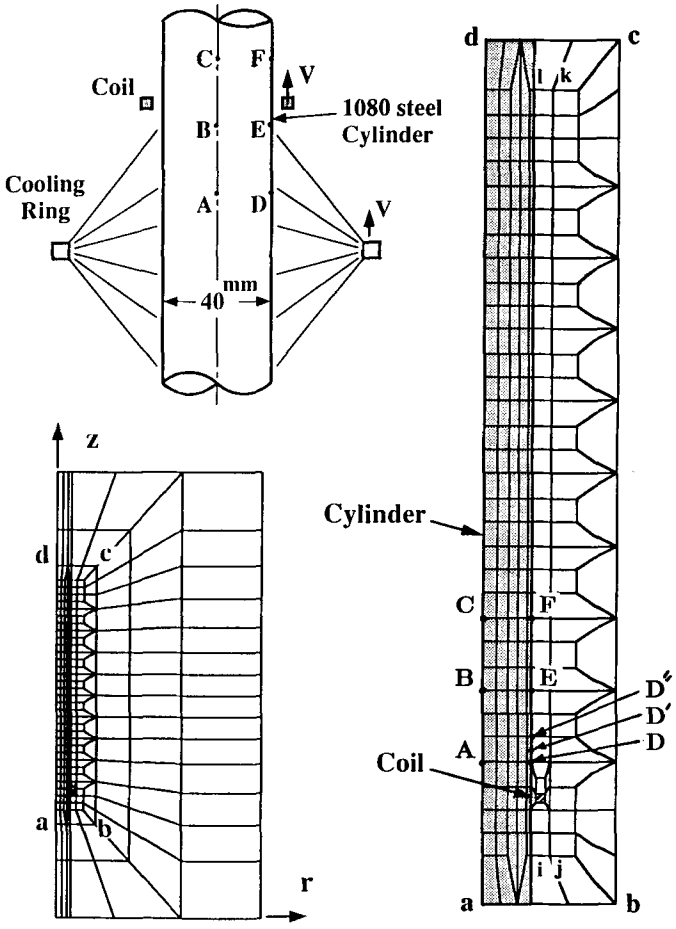

Fig. 5 Geometry and finite-element mesh for the induction heat treatment of an infinitely long 1080 steel cylinder by a moving coil and cooling ring

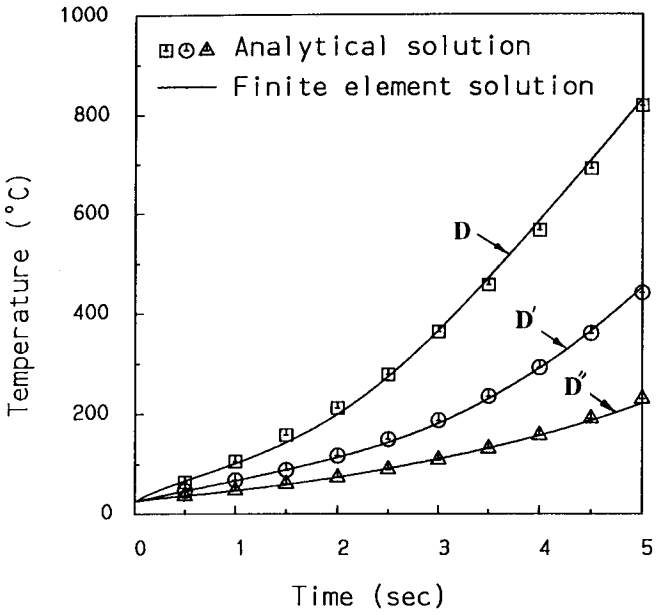

Fig. 6 Temperature-time histories at three points (D, D', and D'') on the surface of the infinitely long cylinder during induction heating by a moving coil

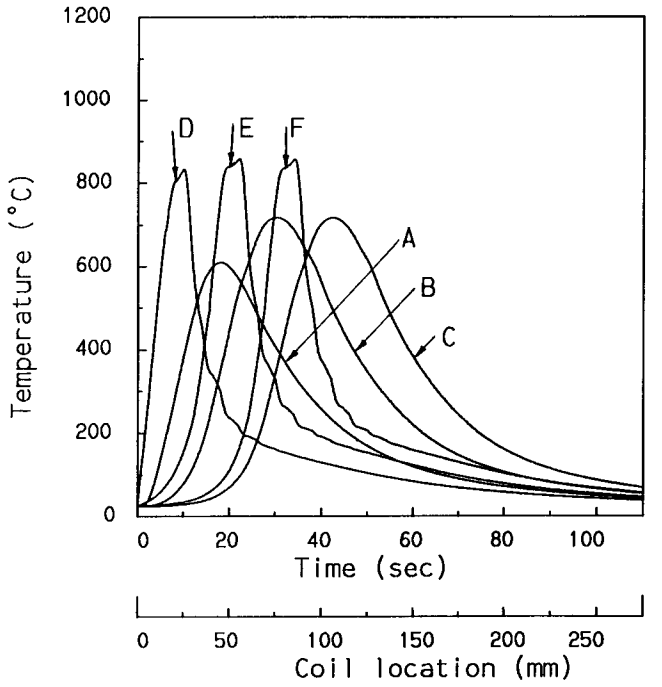

Fig. 7 Temperature-time histories at six points of the infinitely long cylinder during heat treatment by a moving coil and cooling ring. Coil velocity = 2.5 mm/s; current density = 13,800 A/mm^2

temperature had been reached during heating. The martensitic layer (i.e., martensite fraction > 0.5) is seen to extend to a distance of about 5 mm from the cylinder surface. The microstructure within the inner core (r < *4* mm) retains its original pearlite structure. The residual stress distribution (at t = 110 s) along the radius BE (see Fig. 5) is shown in Fig. 9.

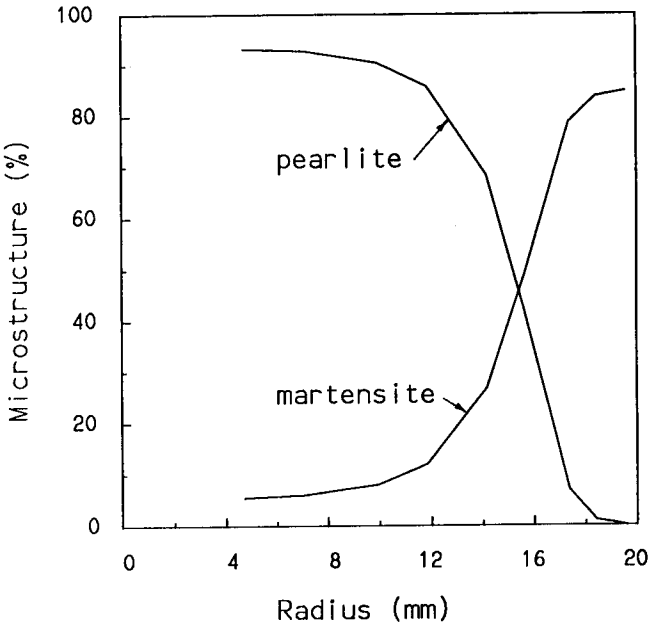

Fig. 8 Microstructure distribution along the radius BE after heat treatment (t = 110 s)

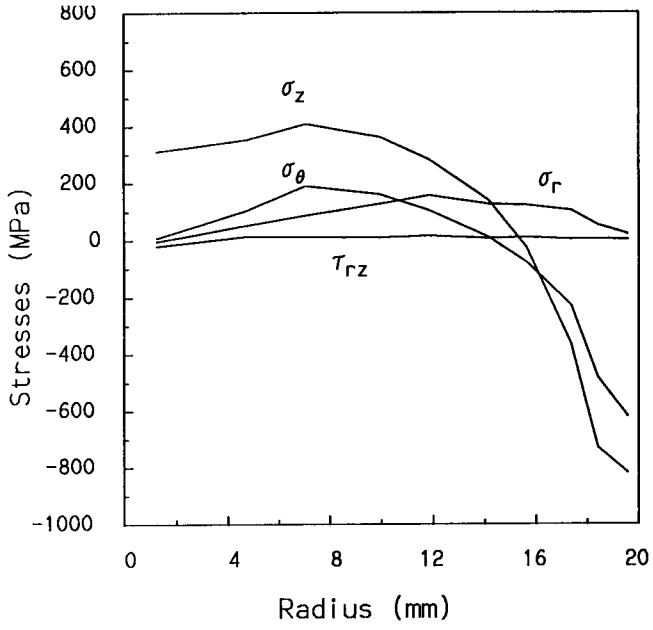

Fig. 9 Residual stress distributions along the radius BE after heat treatment (t = 110 s)

It is of interest to note that three finite-element meshes (236, 265, and 316 elements, respectively) were used to investigate the convergence of results as the mesh was refined. The meshes of 236 and 265 gave two sets of temperature-time curves that were different from the analytical solution in Fig. 6 by less than 8 and 5%, respectively. These two sets of curves are not shown here. The 316-element mesh gave a set of sufficiently accurate temperature-time curves (less than 1% difference) as compared with the analytical solution.

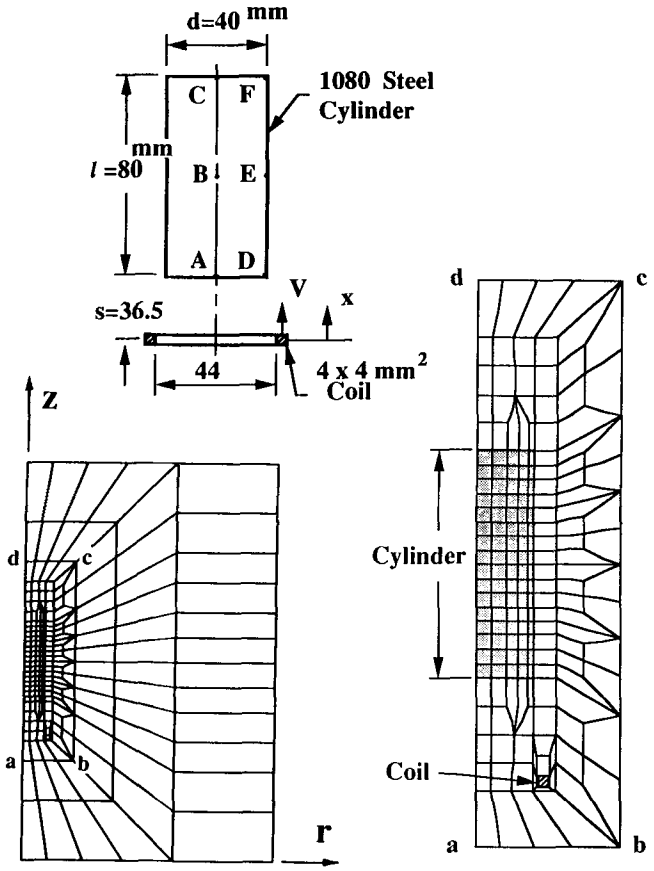

Fig. 10 Geometry and finite-element mesh for a 1080 steel cylinder heated by a moving coil and quenched in a UCON quenchant bath

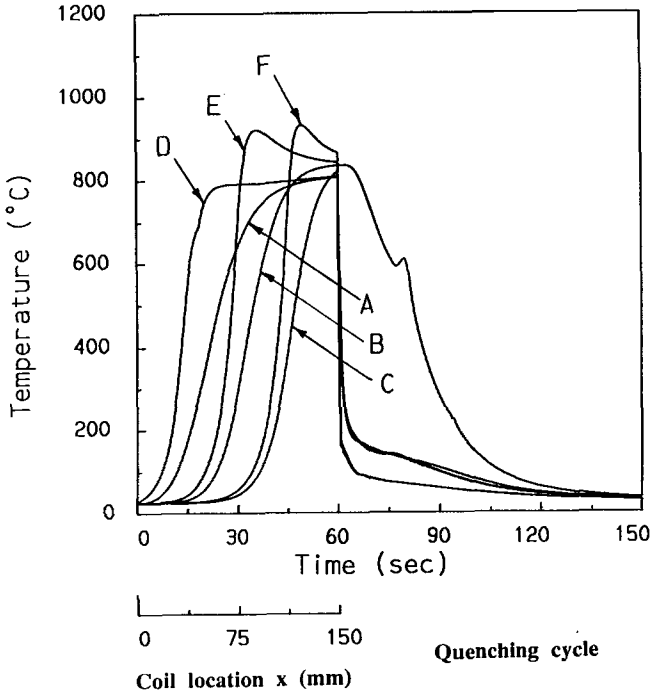

Fig. 11 Temperature-time histories at six points of the finite cylinder during induction heating by a moving coil. Coil velocity = 2.5 mm/s; current density = 13,800 A/mm^2

3.2 *Finite Cylinder Heated by a Moving Coil and Quenched in a Bath*

In the induction heat treatment of workpieces such as piston pins, a cylindrical workpiece of finite length is heated by a moving coil and quenched in a bath. Therefore, the simulation of the induction heating of 1080 steel cylinders, 80 mm in length, by a moving coil and their subsequent quenching in a bath was analyzed. Figure 10 shows the geometries of the cylinder and the coil and their relative initial positions. A mesh for the entire space consisted of 234 eight-node isoparameter elements, as shown in Fig. 10. The cylinder was assumed to be at an initial temperature of 25 °C. The current density and the current frequency in the coil were the same as those in the previous example. The physical and mechanical properties of 1080 steel were assumed to be temperature dependent and the same as those used by Wang et al. (Ref 5). For a coil moving with a velocity of $V = 2.5$ mm/s, the cylinder was heated for a duration of 60 s and then cooled in a UCON-A (UCON is the trade name for widely used commercial quenching fluid) quenchant bath. The convection heat-transfer coefficient for UCON quenchant is temperature dependent, and its values were assumed from Wang et al. (Ref 8). During the heating cycle, the energy losses due to air convection are typically small compared with the heat generated by the eddy current and thus were neglected here.

Figures 11 and 14 show the results of the finite-element simulation. The temperature histories at six points in the cylinder (see Fig. 10 for their locations) during the heat treatment process are shown in Fig. 11. From this it is clear that the austenite transformation temperature of 723 °C has been reached everywhere within the cylinder during heating. The sudden change in the slope of the temperature-time curve at about 620 °C for point B (Fig. 11) during quenching is due to the latent heat released during the pearlitic transformation. Figure 12 shows the microstructure distribution after quenching. The martensite layer (>50% martensite) is seen to extend to a depth of about one-fourth of the cylinder radius after the heat treatment process. Figure 13 shows the residual stress distribution ($t = 150$ s) along the radius BE of the cylinder. The cylinder is under tension in the inner core, with all three stresses (σ_z, σ_r, and σ_θ) being tensile, whereas it is under compression near the surface.

In order to characterize the edge effects in the finite cylinder after induction heat treatment, the residual stress ($t = 150$ s) distributions were plotted along the axis of the cylinder (Fig. 14). Both the radial and hoop stresses are tensile and equal within the cylinder in the region away from the top and bottom surfaces (Fig. 14); however, they change quite rapidly at a distance of about 10 mm from the end surfaces and become compressive near the surface. This is due to the effect of the cylinder end faces.

The effect of coil velocity on the temperature distribution during induction heating was also investigated. The total distance of coil movement was kept constant at 150 mm for this purpose. Figure 15 shows the temperature distribution within

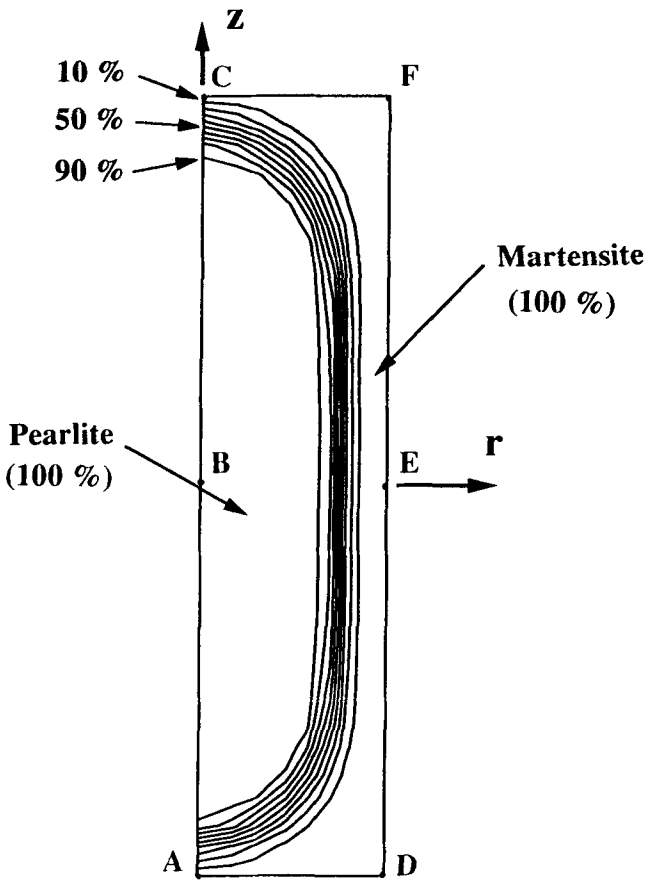

Fig. 12 Fractional contours of pearlite in the heat-treated cylinder

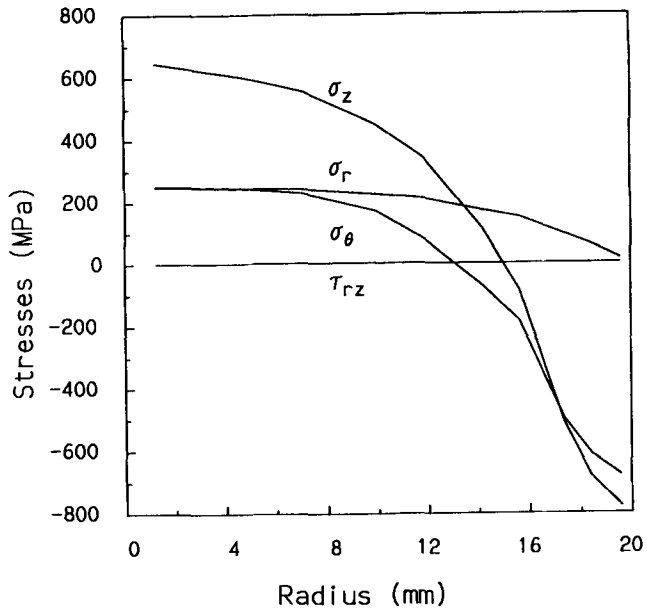

Fig. 13 Residual stress distributions along the radius BE of the cylinder (t = 150 s)

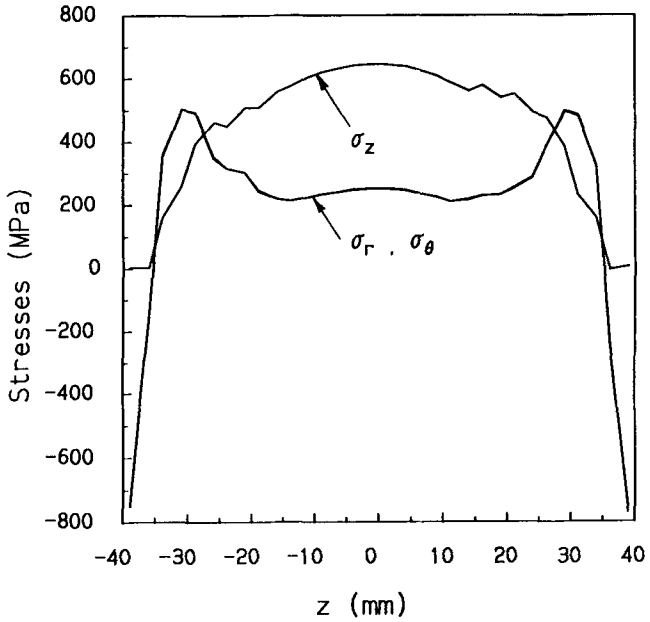

Fig. 14 Residual stress distributions along the cylinder axis after heat treatment (t = 150 s) showing edge effects

80 mm long cylinders after induction heating for two different coil velocities. It is clear that the temperature distribution corresponding to the lower coil velocity is much more uniform than that for a higher velocity. Figure 16 shows the maximum temperature difference (ΔT_{max}) within the cylinders as function of coil velocity for three cylinder of different lengths (40, 60, and 80 mm). These temperature differences were estimated at the end of induction heating. For the cylinders with *L/D* ratios closer to 1, a uniform temperature distribution can be obtained by using a lower coil velocity. When *L/D* increases, a local minimum is observed in ΔT_{max}; this occurs at a velocity of V = 2.5 mm/s for the 80 mm long cylinder (Fig. 16). Although a more uniform temperature distribution can be obtained by using a lower coil velocity (e.g., V = 0.1 mm/s rather than V = 2.5 mm/s), this has the disadvantage that the heating time will be increased by a factor of 25 compared to V = 2.5 mm/s.

3.3 *Induction Heat Treatment of Finite Cylinders by Stationary Solenoidal Coils*

The induction heat treatment of 80 mm long 1080 carbon steel cylinders using multiturn (solenoidal) coils was then analyzed. An objective of this study was to investigate the effect of the coil spacing on the temperature and residual stress distributions developed during heat treatment.

Figures 17 and 18 show the geometries of the cylinder and the two solenoidal coils considered in the heat treatment simulation. Both of the solenoidal coils have 11 turns, and their inner radii are the same (22 mm). However, the spacing between consecutive turns of the coil is constant for the coil shown in Fig. 17 (uniform coil), whereas the one shown in Fig. 18 has a varying spacing between consecutive turns (nonuniform coil). The cross sections of the coils were 4 by 4 mm^2, and the source current frequency was 60 Hz in both cases. The source current densities used with the uniform and nonuniform coils were 1.5 ×

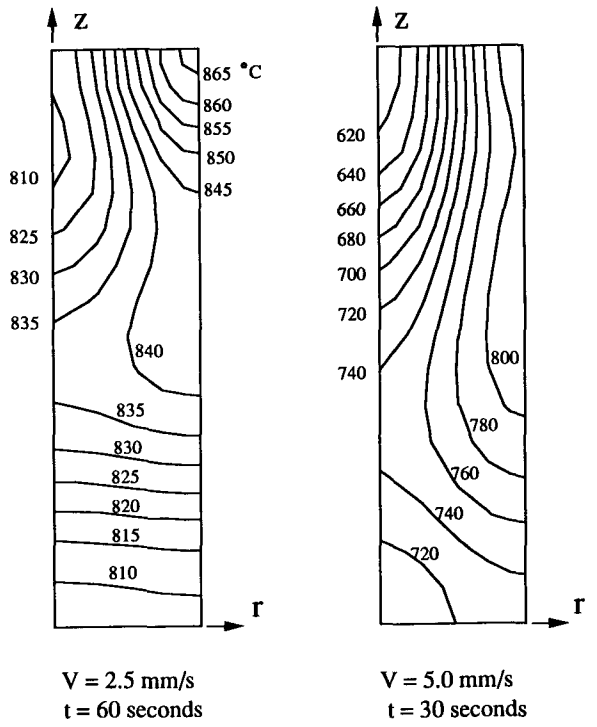

Fig. 15 Effect of coil velocity on temperature distribution

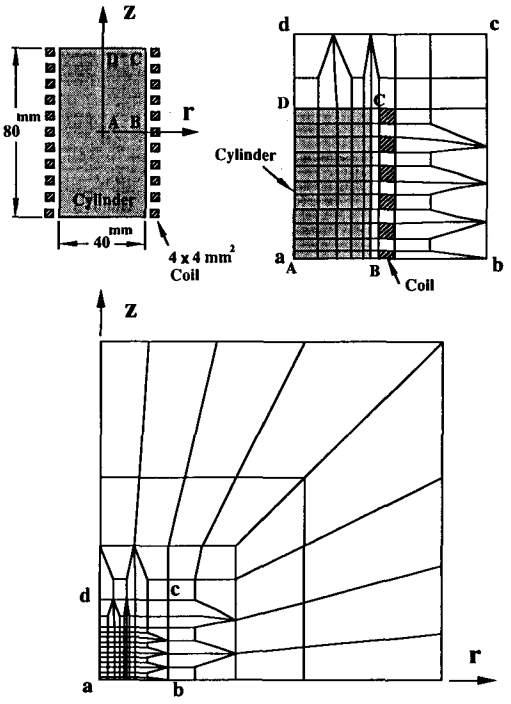

Fig. 17 Geometry and finite-element mesh for a finite cylinder heated by a uniform solenoidal coil

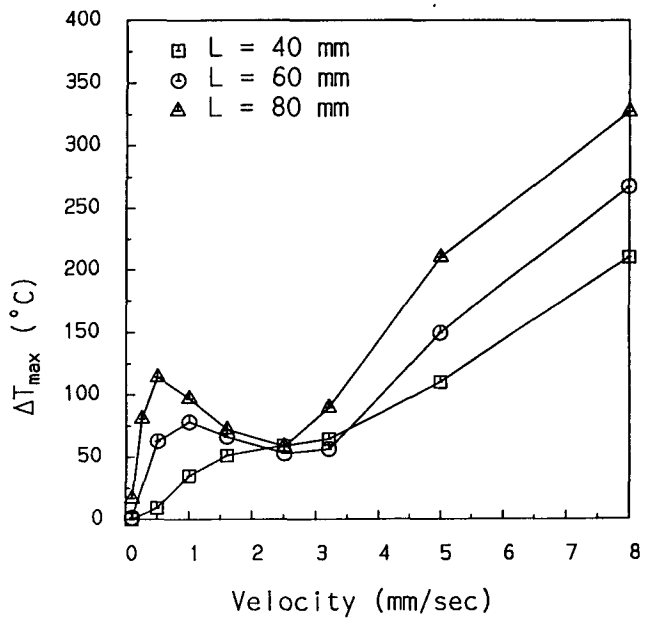

Fig. 16 Variation of the maximum temperature difference (ΔT_{max}) with coil velocity during induction heating. L, cylinder length

10^9 and 1.55×10^9 A/m^2, respectively, so that the average temperature of the workpiece after induction heating for 60 s was about the same in both cases. The material properties of 1080 carbon steel were assumed to be temperature dependent and the same as those used by Wang et al. (Ref 5).

Figures 17 and 18 show the finite-element meshes used in the temperature and residual stress analyses. Meshes with 141 and 157 eight-node isoparametric elements were used to model half of the space with the uniform and the nonuniform coils, respectively. It must be noted that for the uniform coil three meshes of 105, 141, and 210 elements were used and that for the nonuniform coil three meshes of 118, 157, and 224 elements were used. The 141- and 157-element meshes were the coarsest required to obtain sufficiently converged results for the two problems.

Figure 19 shows the temperature distributions within the cylinders after induction heating for 60 s by the two types of solenoidal coils. The temperature distribution in the cylinder heated by the nonuniform coil is seen to be much more uniform than in the cylinder heated by the uniform coil. Also, comparison of the temperature distributions of Fig. 19 with those obtained during induction heating by a moving single coil (see Fig. 15) shows that a more uniform temperature distribution within the cylindrical workpiece can be obtained by using a single coil moving at an appropriate velocity than with a uniform solenoidal coil. Thus, the results show that relatively uniform temperature distributions within workpieces during induction heating can be achieved by adjusting either the velocity of a moving coil or the spacing of a stationary solenoidal coil.

Figure 20 shows the residual stress distributions along the radius AB in the cylinders after heat treatment. The stresses were calculated using the finite-element method. It was assumed that the heated cylinders were quenched in a bath of UCON-A; the convection coefficient for UCON-A was the same as in the previous example and taken from Wang et al. (Ref 8). There appears to be little difference in the residual stresses produced by the two types of solenoidal coils. This example suggests that the simulation procedures could be usefully applied in coil design.

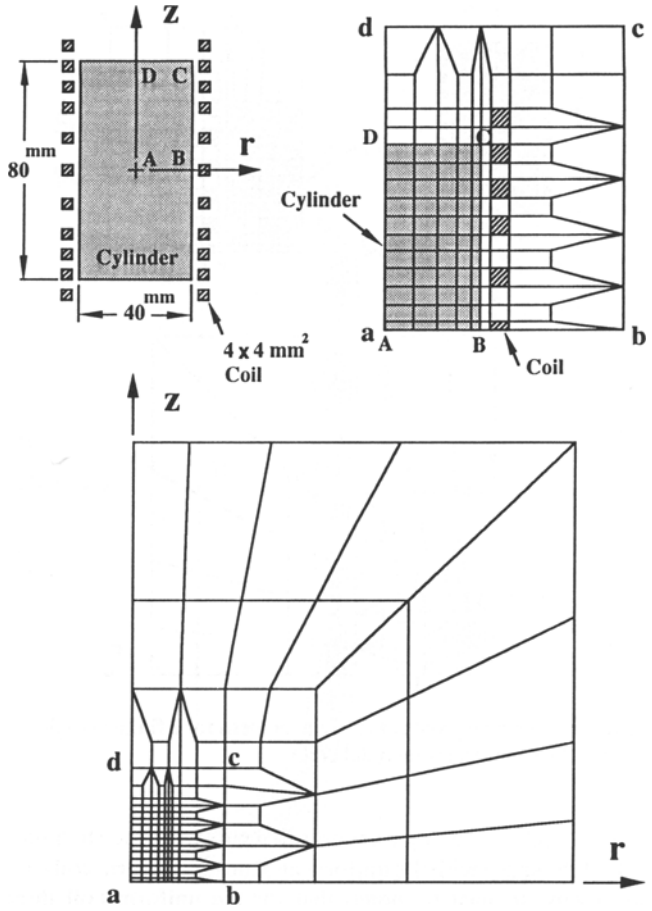

Fig. 18 Geometry and finite-element mesh for a finite cylinder heated by a nonuniform solenoidal coil

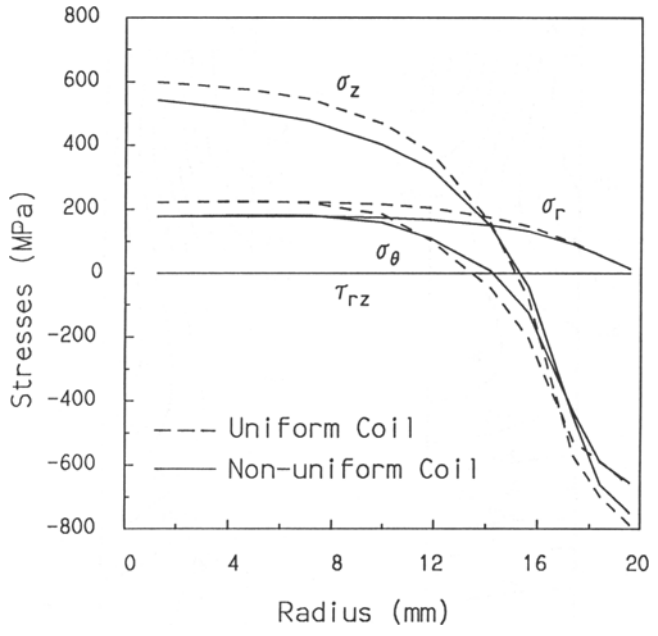

Fig. 19 Temperature contours in the finite cylinder after induction heating by uniform and non-uniform solenoidal coils (t = 60 seconds).

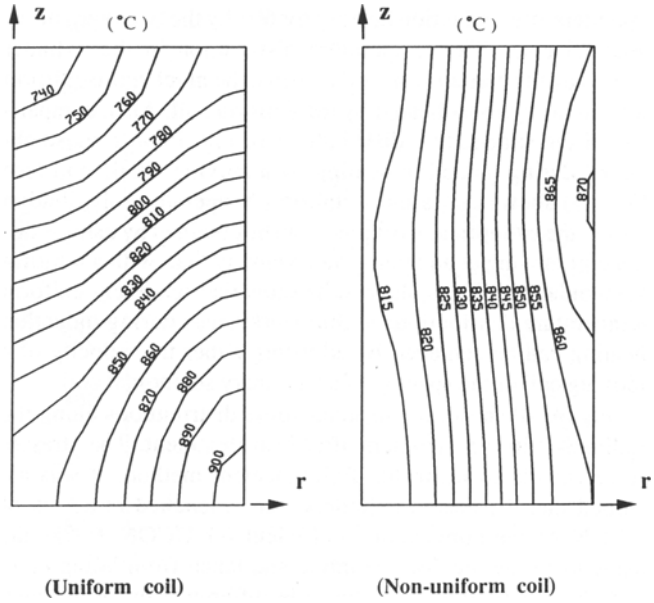

Fig. 20 Residual stress distributions along the radius AB of the heat-treated cylinders.

4. Conclusion

A finite-element procedure with a remesh scheme has been developed and applied to simulate moving induction heat treatment problems. The temperature, microstructure, and residual stress distributions developed in 1080 steel cylinders after induction heat treatment have been calculated. The effect of coil velocity and coil spacing (for multiturn solenoidal coils) on temperature distributions during induction heating has also been analyzed. Analytical solutions for the magnetic vector potential and temperature distribution have been derived using Green's function methods for some moving coil problems; these solutions have enabled validation of the finite-element analysis of moving induction heating. The simulation procedure can serve as a useful design tool in induction coil design and in the selection of process parameters.

Acknowledgments

This work was supported by grants from the National Science Foundation (CDR 8803017) to the Engineering Research Center for Intelligent Manufacturing Systems and the Computer Integrated Design Manufacturing and Automation Center (CIDMAC) at Purdue University. The authors wish to thank Wayne Eckerle, Bill Grant, Carl Musolff, and Ted Winterrowd of Cummins Engine Company and Bob Kobylarz, Tom Strong, and Greg Williamson of Atlas Company for valuable discussions at various stages of the study.

References

1. C.V. Dodd and W.E. Deeds, "Analytical Solution to Eddy-Current Probe Coil Problems," Report ORNL-TM-1987, 1967
2. J. Donea, S. Giuliani, and A. Philippe, Finite Elements in the Solution of Electromagnetic Induction Problems, *Int. J. Numer. Meth. Eng.*, Vol 8, 1974, p 359-367

3. M.V.K. Chari, Finite-Element Solution of the Eddy-Current Problem in Magnetic Structures, *IEEE Trans. Power Appl. Sys.*, Vol PAS-93 (No. 1), 1974, p 62-72
4. M. Melander, Theoretical and Experimental Study of Stationary and Progressive Induction Hardening, *J. Heat Treat.*, Vol 4, 1985, p 145-166
5. K.F. Wang, S. Chandrasekar, and H.T.Y. Yang, Finite Element Simulation of Induction Heat Treatment, *J. Mater. Eng. Perform.*, Vol 1 (No. 1), 1992, p 97-112
6. M. Melander, Computer Predictions of Progressive Induction Hardening of Cylindrical Components, *Mater. Sci. Technol.*, Vol 1, 1985, p 877-882
7. C.V. Dodd, "Solutions to Electromagnetic Induction Problems," Report ORNL-TM-1842, 1967
8. K.F. Wang, S. Chandrasekar, and H.T.Y. Yang, An Efficient 2D Finite Element Procedure for the Quenching Analysis with Phase Change, *ASME J. Eng. Ind.*, Vol 115 (No. 1), 1993, p 124-138
9. M. Avrami, Kinetics of Phase Change I, *J. Chem. Phys.* Vol 7, 1939, p 1103
10. M. Avrami, Kinetics of Phase Change II, *J. Chem. Phys.*, Vol 8, 1940, p 212
11. F.M.B. Fernandes, S. Denis, and A. Simon, Mathematical Model Coupling Phase Transformation and Temperature Evolution during Quenching of Steels, *Mater. Sci. Technol.*, Vol 1, 1985, p 838-844
12. D.P. Koistinen and R.E. Marburger, A General Equation Prescribing the Extent of the Austenite-Martensite Transformation in Pure Iron-Carbon Alloys and Carbon Steels, *Acta Metall.*, Vol 7, 1959, p 59
13. B. Buchmayr and J.S. Kirkaldy, Modeling of the Temperature Field, Transformation Behavior, Hardness and Mechanical Response of Low Alloy Steels during Cooling from the Austenite Region, *J. Heat Treat.*, Vol 8 (No. 2), 1990, p 127-136